Journal of Materials Chemistry A

Accepted Manuscript

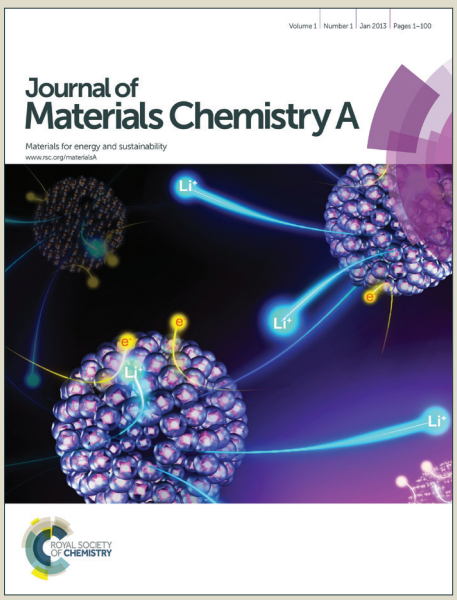

ROYAL SOCIETY OF CHEMISTRY

www.rsc.org/materialsA

Journal of Materials Chemistry A

Cite this: DOI: 10.1039/c0xx00000x

www.rsc.org/xxxxxx

Full Paper

BiOBr Visible-Light Photocatalytic Film in Rotating Disk Reactor for Organics Degradation †

Yuning Huo*, Rujing Hou, Xiaofang Chen, Haibo Yin, Yuan Gao, and Hexing Li*

Received (in XXX, XXX) Xth XXXXXXXXX 20XX, Accepted Xth XXXXXXXXX 20XX
DOI: 10.1039/b000000x

A facile solvothermal approach assisted with [C_{16}mim]Br ionic liquid for the preparation of BiOBr visible-light photocatalytic films was developed. BiOBr film with uniformly assembled nanosheets was stably grown on the pretreated soda glass substrate *via* the Bi-O-Si bond. The rotating disk reactor coated with BiOBr film was designed to effectively avoid the light shielding from color solution. BiOBr film obtained with [C_{16}mim]Br ionic liquid presented the improved visible-light photcatalytic degradation rate of organics in wastewater, especially at the high concentration of organic dyes with deep color. The stable combination of BiOBr film with the substrate, the enhanced light harvesting owing to multiple reflections within the network of BiOBr nanosheets, the high separation efficiency of photo-induced charge carriers, the fast adsorption rate and the efficient utilization of light in rotating disk reactor, simultaneously played the important roles during the degradation process, leading to the applicable future for the practical wastewater treatment.

1. Introduction

Photocatalysis technology has attracted more attentions in recent years for the removal of global environmental pollutants. Various photocatalysts in the form of powder and film have been explored in order to meet the requirements of the high efficient photocatalysis and the solar light utilization.[1, 2] The photocatalytic efficiency is mainly dependent on photoelectrons-hole recombination, the photocatalyst activation by sunlight, and the stability of photocatalyst. Although TiO_2 photocatalyst has been widely applied owing to its advantages of cheapness, non-toxicity and stability, the practical application of TiO_2 is still limited due to no light absorption within the visible-light region and the low quantum efficiency.[3, 4] Besides of the modification of TiO_2, many efforts have been devoted to designing the novel non-TiO_2 semiconductors with intrinsic nature of visible-light harvesting.[5, 6] Bismuth oxybromide (BiOBr) photocatalyst with the layered crystal structure of tetragonal matlockite[7, 8] has visible-light irradiation.[9-11] Up to date, various approaches raised a surge of interest owing to its easy preparation and stable property under including hydrolysis[12], reverse micro-emulsion[13], solvothermal[14, 15] and microwave[16] processes have been carried out for the preparation of BiOBr powder with different morphologies such as flower-like microspheres and nano-scale particles. However, the application of powder BiOBr photocatalyst is still restricted due to the difficult separation and reuse. More importantly, during the photocatalytic degradation process, the photocatalysts could not be sufficiently irradiated by sunlight due to the light-shielding effect from the solution, especially from the color solution containing organic dye pollutants. Our preliminary test demonstrated that the sunlight can reach only about 1 mm depth in 50 mg/L aqueous solution. Therefore, it is essential to prepare the BiOBr film coated on the substrate and design the efficient photocatalysis reactor to enhance the light utilization. Although a variety of methods have been developed to coat uniform TiO_2 film onto the different substrates[17-19], the BiOBr film was still in need of development since its layered tetragonal structure results in the poor interaction with the substrate and thus detaches easily. Herein, we reported a facile approach to coat BiOBr film onto the glass substrate by solvothermal route assisted with 1-hexadecyl-3-methylimidazolium bromide ([C_{16}mim]Br, see the following chemical structure) ionic liquid (IL) followed by adhering onto a disk. The BiOBr film with uniformly assembled nanosheets was successfully grown on the pretreated glass substrate to enhance the light harvesting *via* multiple reflections and it was utilized in

The Education Ministry Key Lab of Resource Chemistry, Shanghai Key Laboratory of Rare Earth Functional Materials, Shanghai Normal University, Shanghai 200234, China. E-mail: Hexing-li@shnu.edu.cn, huoyuning@shnu.edu.cn; Fax: 86-21-6432-2272; Tel: 86-21-6432-1673.

† Electronic supplementary information (ESI) available: See DOI: 10.1039/c0xx00000x

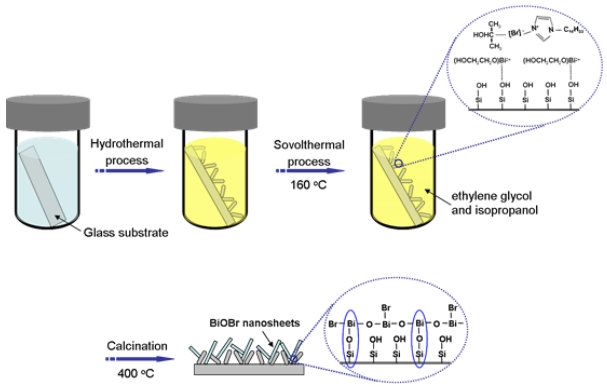

Scheme 1 Plausible procedure of the formation of BiOBr film.

the photocatalysis reactor with rotating disk[20] (Fig. S1), which could completely exclude the light-shielding effect from color solution by rotating the disk. As a result, the photocatalytic rotating reactor containing the BiOBr film exhibited high photoactivity and durability under visible light irradiation, especially for the degradation of organic dye pollutants, showing good potential in cleaning wastewater from dying industries. Additionally, the effect of [C_{16}mim]Br IL, which acted as both the Br source and structure direction agent, to the growth of BiOBr film were investigated.

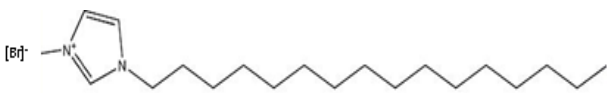

2. Experimental details

2.1 Preparation of BiOBr films

The BiOBr film coated on the glass substrate (2.5 × 4.4 cm) was synthesized through a solvothermal route (see Scheme 1). In a typical process, 0.12 g $Bi(NO_3)_3{\cdot}5H_2O$ was dissolved into 40 mL solution mixed with the optimal ratio of 5.0 mL ethylene glycol and 35 mL isopropanol[14] under vigorously stirring at 30 °C for 30 min to achieve a transparent solution. The [C_{16}mim]Br IL was then added with Bi/Br molar ratio of 1 : 2 and stirred vigorously for 1.0 h. The obtained solution was transferred into a 50 mL Teflon-lined stainless steel autoclave containing one vertically placed soda glass plate pre-treated *via* hydrothermal procedure according to the previous report.[21] Then, the autoclave was sealed and maintained at 160 °C for various time interval followed by naturally cooling to room temperature. The as-prepared films were washed with ethanol and deionized water for at least 3 times and dried at ambient temperature for 1.0 h. Finally, the films were calcined at different temperatures for 4 h to improve the crystallization of catalyst and remove the organic residuals. The obtained samples were denoted as BOB-X-Y, where X and Y represented the solvothermal time (h) and calcination temperature (°C), respectively.

For comparison, BOB-8-400(M) film was obtained *via* substituting [C_{16}mim]Br IL with the mixture of 1-hexadecyl-3-methylimidazolium nitrate ([C_{16}mim][NO_3]) IL and NaBr in BOB-8-400 film. The films prepared using cetyltrimethylammonium bromide (CTAB) instead of [C_{16}mim]Br IL were referred to BOB-8-400(C). The average amount of different films on glass substrate was similar to that of BOB-8-400. BOB-8-400(P) was the BiOBr powder achieved *via* the same route as preparing BOB-8-400 film without the glass substrate.

2.2 Characterization

The structure was examined by X-ray diffraction (XRD, Rigacu D/Max-2000), selected area electronic diffractions (SAED, JEM-2010) and Fourier transform infrared (FTIR) (NEXUS 470). The crystallite size was calculated based on the Scherrer equation ($D = K\lambda/\beta\cos\theta$). Surface morphologies were observed by scanning electron microscopy (FESEM, HITACHI S-4800). X-ray photoelectron spectroscopy (XPS, Versa Probe PHI 5000) was employed to determine surface electronic states. The shift of the binding energy due to relative surface charging was corrected using the C1S level at 284.8 eV as an internal standard. The optical property was analyzed by both UV-vis diffuse reflectance spectra (DRS, MC-2530) and photoluminescence spectra (PLS, Varian Cary-Eclipse 500). The measurement system of surface photovoltage spectroscopy (SPS) was assembled by a source of monochromatic light, a light chopper (SR540, Stanford) and a lock-in amplifier (SR830-DSP, Stanford). A 500 W xenon lamp (CHF XM500W, Stusttech) and a double-prism monochromator (Omini-500, Zolix) were combined to provide monochromatic light. A chopping frequency of 23 Hz was utilized. The photovoltaic cell had a sandwich structure of ITO-sample-ITO. The contact angle of water droplet on the film was measured by the sessile drop method at 20 °C on a JC2000D contact angle analyzer. All measurements were performed at five spots on the surfaces. The electron spin resonance (ESR) spectra were detected on a Bruker model A300 spectrometer under visible light irradiation (λ> 420 nm) with the settings of center field (3512.48 G), microwave frequency (9.86 GHz) and power (6.35 mW). The radicals capture agent was 5,5-Dimethyl-l-pyrroline-N-oxide (DMPO) dissolved in distilled water (for ·OH) or methanol (for $\cdot O_2$), respectively. Zeta potential was measured by Malvern Zetasizer Nano ZS90.

2.3 Adsorption test

The adsorption ability of different samples was investigated *via* uniformly localizing four glass sheets (each size = 2.5 × 2.2 cm) coated with BiOBr film on the rotating disk reactor[20] with plexiglass disk (Fig. S1) in the dark. The diameter of disk was 81 mm. It was immerged into 55 mL probe solution with different organics at 30 °C, including rhodamine B (RhB), methylene blue (MB), methyl orange (MO) and toluene. 57 % surface area of the disk was exposed to the air. The preliminary tests demonstrated a good linear relationship between the light absorbance and the concentration of organic compounds. At given time intervals, the initial concentration of organics (C_0) and concentration during the adsorption process (C) were measured on a UV-vis spectrophotometer (UV-7502PC, XinMao Instrument Co. Ltd, Shanghai) to calculate the adsorption rate, according to the light absorbance at the characteristic peak of 553 (RhB), 664 (MB), 464 (MO) and 201 nm (toluene), respectively. The toluene in aqueous solution was extracted by hexane before the measurement of light absorbance.

2.4 Photocatalysis test

The rotating disk reactor in Fig. S1 was used to evaluate the activity of BiOBr films in photocatalytic degradation of various organics in wastewater at 30 °C. Four glass plates (each size = 2.5 × 2.2 cm) coated with BiOBr films were uniformly localized on the disk and then immerged into 55 mL probe solution of different organics with 57 % surface area exposed to the air. The disk was rotated for 30 min in dark at the speed of 90 rpm to achieve adsorption-desorption equilibrium. Then, the reaction was started by illuminating the rotating disk with a 300 W xenon lamp (CHF-XM500, light intensity = 600 mW/cm^2) located at 10

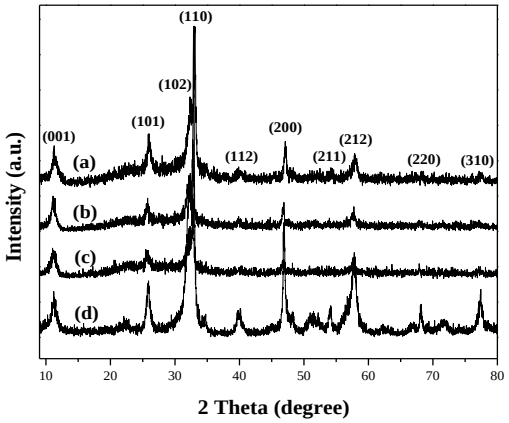

Fig. 1 XRD patterns of (a) BOB-8-400, (b) BOB-8-400(C), (c) BOB-8-400(M), and (d) BOB-8-400(P) samples.

cm away. To make sure that the photocatalytic reaction was really driven by visible-light, all the UV lights with the wavelength less than 420 nm were removed by a glass filter (JB-420). At given time intervals, the concentration of dye compound during the degradation process was measured on the UV-vis spectrophotometer to calculate the degradation rate. The active species during the photocatalytic reaction were determined by additionally dissolving 0.050 mmol trapping agents including EDTA, $AgNO_3$, tert-butyl alcohol (TBA) and benzoquinone (BQ), which could capture photo-generated holes, photo-generated electrons, ·OH radical and $\cdot O_2^-$ radical, respectively. The reproducibility of the results was checked by repeating the experiments at least three times and was found to be within acceptable limits (±5%). The durability of the films was measured according to the following procedure. After each run of photocatalysis reactions, the films were washed with distilled water for 3 times and dried at 100 °C for 12 h. Then, each recycling test was conducted under the same conditions for 3 h and the RhB photodegradation rate was determined to show the change of activity.

3. Results and discussion

3.1 Structure characteristics

XRD patterns in Fig. 1 revealed that all of BOB-8-400, BOB-8-400(C), BOB-8-400(M) and BOB-8-400(P) samples displayed the pure BiOBr tetragonal crystal phase (JCPDS 09-0393). Comparing to the untreated soda glass substrate, continuous three-dimensional porous network displayed in the soda glass substrate pretreated under hydrothermal conditions[21, 22] (see FESEM images in Fig. S2). Such rough glass surface was essential for the steady growth of BiOBr film since BiOBr film could not be coated onto the untreated glass substrate. As shown in FESEM images (Fig. 2), BOB-8-400 obtained with the assistance of $[C_{16}min]Br$ IL showed that the glass surface was uniformly covered by the BiOBr film with thickness around 810 nm. Such a film was comprised of vertically aligned BiOBr nanosheets with the average thickness about 26 nm. In contrast, BOB-8-400(P) powder obtained in the absence of the glass substrate was present in flower-like microspheres, obvously due to the spontaneous gathering of BiOBr nanosheets similar to those observed in BOB-8-400. BOB-8-400(C) prepared using CTAB instead of $[C_{16}min]Br$ IL also displayed the flower-like morphology constructed by the smaller nanosheets, which could not form the uniform BiOBr film onto the glass substrate. By using the mixture of $[C_{16}mim][NO_3]$ and NaBr instead of $[C_{16}min]Br$ IL, the as-prepared BOB-2-8-400(M) showed the assembly of BiOBr nanosheets onto the glass substrate. However, the ordering degree of assembling BiOBr nanosheets was poor in comparison with that in BOB-8-400, leading to the relatively un-uniform BiOBr film. These results demonstrated that all the BiOBr were present in nanosheets with similar shapes regardless of the Br resource, which could be attributed to the same tetragonal crystal. The $[C_{16}min]^+$ IL is essential for the horizontal assembly rather than gathering of BiOBr nanosheets onto the glass substrate to form BiOBr film. Meanwhile, the cooperative effect between $[C_{16}min]^+$ and its connecting Br^- would promote ordering degree in assembling BiOBr nanosheets, leading to the uniform BiOBr film.

Calcination at the temperature from 350 to 400 °C promoted the crystallization and growth of BiOBr crystals into well-defined nanosheets in the BOB-8-400. However, further increase of calcination temperature from 400 to 450 °C resulted in the BiOBr decomposition, together with the formation Bi_2O_3, corresponding to the damage of uniform BiOBr film and the slight increase in film thickness due to the particle re-arrangement (see the XRD patterns and FESEM images in Fig. S3 and S4). Prolonging the solvothermal time from 4 to 12 h had no significant effect on either the crystallization of the BiOBr crystals (see the XRD patterns in Fig. S5) or the film thickness (see Fig. S6). However, the density of BiOBr nanosheets on the glass substrate increased with the increase of solvothermal time since more BiOBr nanosheets were generated and assembled onto the glass substrate.

XPS spectra (Fig. S7) revealed that the binding energy of Br 3d in the $[C_{16}mim]Br$ IL shifted negatively by about 0.8 eV after being dissolved in isopropanol and coated onto the glass substrate, indicative of the change of $[C_{16}mim]Br$ structure in the isopropanol solution and no significant interaction between $[C_{16}mim]Br$ and the glass surface. Meanwhile, FTIR spectra in Fig. S8 showed that, when the $[C_{16}mim]Br$ was dissolved in isopropanol, the stretching vibration of N=C-N bond (1571 cm^{-1}) in imidazole ring tend to be weaker, but the stretching vibration of C=N-C bond (1393 cm^{-1}) to be stronger. It could be attributed to the change of electron cloud density in the imidazole ring, possibly due to the appearance of bending vibration of C-H bond in N=C, corresponding to the vibration bands at 956 and 817 cm^{-1}, respectively.[23, 24] It could be confirmed as the result of the interaction with isopropanol, inducing the slow releasing of Br^- during the formation of the BiOBr nanosheets (see Scheme 1). In comporison, both of the solid $[C_{16}mim]NO_3$-NaBr mixture and the solid CTAB was quite similar to those being dissolved in

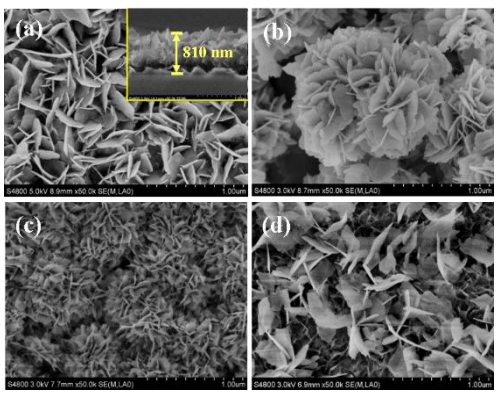

Fig. 2 FESEM morphologies of (a) BOB-8-400 with the cross section, (b) BOB-8-400(P), (c) BOB-8-400(C) and (d) BOB-8-400(M) samples.

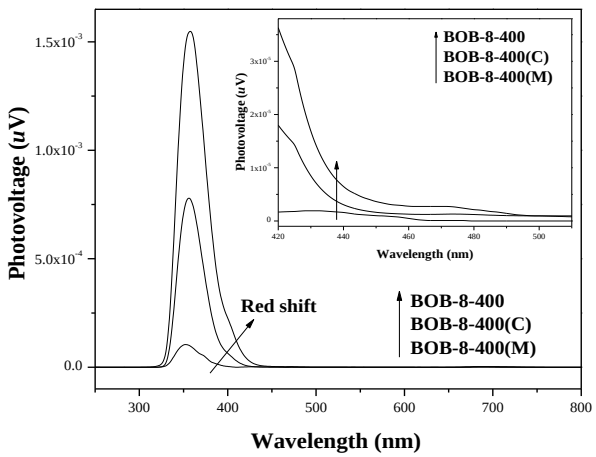

Fig. 3 SPS spectra of different samples. The insert was the SPS spectra in visible light region.

isopropanol, indicative of no significant interaction between either $[C_{16}mim]NO_3$ or CTAB with isopropanol. Thus, the Br^- could be released quickly, leading to the un-uniformly growth of BiOBr nanosheets in BOB-8-400(M) and BOB-8-400(C). Additionally, the glass substrate without pretreatment could not induce the growth of BiOBr nanosheets on it, obviously owing to the absence of Si-OH on the surface. The combination of BiOBr nanosheets with the pretreated glass substrate was investigated by comparing BOB-8-400, BOB-8-400(P) and BOB-8-400(2), which was obtained by coating BiOBr film onto the glass substrate twice. The FESEM morphology and XRD patterns in Fig. S9 revealed that BOB-8-400(2) showed significant increase of film thickness from 810 nm to 1.13 um with the enhanced BiOBr crystallization, but the shape of BiOBr nanosheet remained almost constant. From Fig. S10, the characteristic FTIR peak of Bi-O-Si bond at 528 cm^{-1} [25] was absent in BOB-8-400(P) and BOB-8-400(2) but obviously presented in BOB-8-400, comparing to that in Bi_2SiO_5. It implied that the twice preparation process was difficult to generate the firm combination of BiOBr nanosheets with glass substrate. XPS spectra in Fig. S11 further confirm the combination of BiOBr nanosheets with glass substrate. In comparison with that in both BOB-8-400(P) and BOB-8-400(2), the Bi_{4f} shift of binding energy in BOB-8-400 with the same peak position as that of Bi_2SiO_5[26] was obviously attributed to the strong combination with glass substrate *via* forming the Bi-O-Si bond. The Si_{2p} peak at 103.1 eV[27] was only presented in BOB-8-400. The O_{1s} peak in BOB-8-400 could be assigned to the existence of both SiO_2 (532.4 eV) and BiOBr (529.8 eV). However, only O_{1s} peak of BiOBr could be found in BOB-8-400(2) with the shift to 530.1 eV since the second coated BiOBr film was mainly covered onto the original BiOBr film rather than the glass substrate. Thus, it could be confirmed that the BiOBr nanosheet in BOB-8-400 was stable chemically combined with the glass substrate, induced by the slow-releasing of Br^- *via* the interaction of $[C_{16}min]Br$ IL with isopropanol. Additionally, the formation of BiOBr compound rather than Bi_2O_3 or metallic Bi[28] in BOB-8-400 was also demonstrated, in accordance with the afore-mentioned XRD results.

According to the above results, the plausible formation process of BiOBr films could be proposed in Scheme 1. At first, the pretreated soda glass substrates provided the surface Si-OH bond and the continuous porous three-dimensional network for the crystal growth of BiOBr film. Then, the stably linearly-aligned alkoxides ($Bi(OCH_2CH_2OH)^{2+}$) was formed by the coordination of ethylene glycol with Bi^{3+} [29-30] and combined with Br^- slow-released from $[C_{16}min]Br$-isopropanol interaction, leading to the formation of BiOBr lamellas. The mixed glycol and isopropanol might serve as the soft template structurally directing the BiOBr crystal growth into nanosheets.[14] Finally, the stable interaction of BiOBr nanosheets with the glass substrate was formed *via* the Bi-O-Si bond and prevented the formation of flower-like morphology on the substrate.

3.2 Optical properties

UV-vis DRS spectra (Fig. S12) demonstrated that all the BiOBr films displayed the spectral response in visible area corresponding to the narrow energy band gap around 2.8 eV, in good accordance with the theoretical value of the BiOBr tetragonal crystals.[8] BOB-8-400, BOB-8-400(M) and BOB-8-400(C) exhibited similar light absorbance, indicating that gathering morphologies of BiOBr nanosheets onto the glass substrate had no significant influence on the light harvesting ability. However, BOB-8-400 displayed much stronger light absorbance than BOB-8-400(P), suggesting that the combination of BiOBr nanosheets with the glass substrate could enhance the light reflections. BOB-8-400(2) exhibited further enhanced light absorbance owing to the increase of BiOBr nanosheets on the glass substrate.

The SPS measurement was a well-established contactless and nondestructive technique for detecting the illumination-induced changes in the surface photovoltage of semiconductor.[31] Although the similar light harvesting abilities, BOB-8-400 exhibited much stronger SPS response than either BOB-8-400(M) or BOB-8-400(C) (Fig. 3). Meanwhile, a red shift of photovoltage response threshold of BOB-8-400 indicated the favored electron excitation from valence to conduction band to generate more photo-charges.[32] It also related to the higher separation efficiency of photo-induced charge carriers and the stronger surface charge transfer under light irradiations[33, 34], which was consistent with the PL spectra. As shown in Fig. S13, BOB-8-400 displayed much weaker PL intensity around 426 nm than either BOB-8-400(M) or BOB-8-400(C), showing the lower recombination rate of photo-induced electrons and holes since the ordering assembly of BiOBr nanosheets onto the glass substrate facilitated the transfer of electrons and diminished the recombination with holes.

3.3 Adsorption property

Fig. 4 revealed the RhB and benzene adsorption on different BiOBr films in the rotating disk reactor. No significant adsorption was observed on the blank rotating disk due to the extremely low surface area. The RhB adsorption capacity decreased in the order of BOB-8-400, BOB-8-400(M) and BOB-8-400(C), which was consistent with the change of S_{BET} (30.4, 27.8 and 14.2 m^2/g). Meanwhile, BOB-8-400 displayed more rapid adsorption than the BOB-8-400(M), which could be mainly attributed to the stronger surface hydrophilicity (see the smallest contact angle in Fig. S14), taking into account of the similar surface Zeta potentials (Fig. S15). Although the largest contact angle, the BOB-8-400(C) exhibited similar adsorption rate for RhB to the BOB-8-400, which could be attributed to its more negtive surface Zeta potential. In comparison, BOB-8-400, BOB-8-400(M) and BOB-8-400(C) showed the similar adsorption rate of benzene (uncharged species), further confirming the significant effect of surface charges. It was also found that BOB-8-400 exhibited higher adsorption rate for RhB and MB than for MO (Fig. S16), obviously due to the negative surface Zeta potential, taking into account that both RhB and MB are cationic while MO is anionic (see molecular structure in Scheme S1).

3.4 Photocatalytic performance

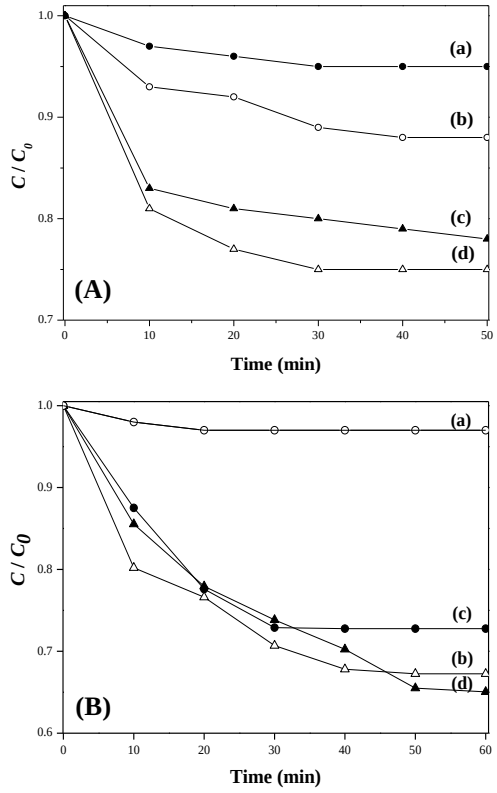

Fig. 4 Adsorption property of (A) RhB and (B) benzene in the case of (a) no catalyst on disk, (b) BOB-8-400(M), (c) BOB-8-400(C) and (d) BOB-8-400 on rotating disk. Adsorption conditions: four glass plates (each size = 2.5 × 2.2 cm) coated with catalysts on the disk, 55 mL 13 mg/L RhB or 10 mg/L benzene aqueous solution, reaction temperature = 30 °C, rotating speed = 90 rpm.

The visible-light driven photocatalytic degradation of RhB was used as a probe for testing the activity of BiOBr on the rotating disk. From Fig. S17, the degradation of RhB in the absence of photocatalyst could be neglected.

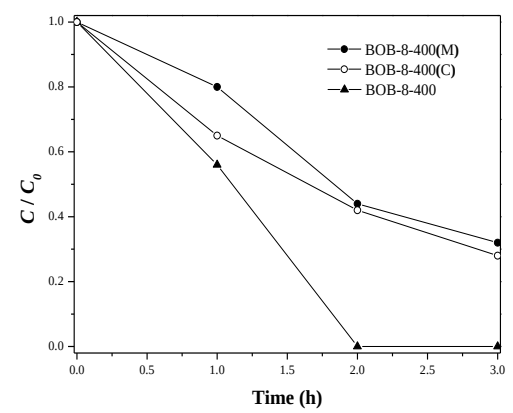

Fig. 5 Photodegradation of RhB on different film. Reaction conditions: four glass plates (each size = 2.5 × 2.2 cm) coated with catalysts on the disk, 55 mL 10 mg/L RhB aqueous solution, reaction temperature = 30 °C, one 300 W Xe lamp (light intensity = 600 mW/cm^2, λ > 420 nm), rotating speed = 90 rpm.

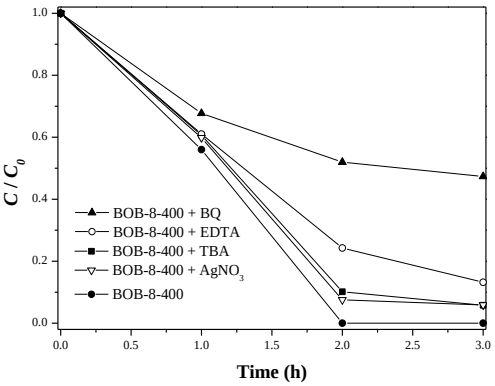

Fig. 6 Reaction process for photocatalytic degradation of RhB on BOB-8-400 film with and without trapping agents. Reaction conditions were given in Fig. 5.

With the increase of solvothermal time, the activity of the BiOBr film coated on the rotating disk first increased and then decreased, and BOB-8-400 exhibited the highest activity. The activity increased with the increasing solvothermal time from 4 to 8 h since more BiOBr nanosheetswere assembled onto the glass substrate. However, further increase in the solvothermal time from 8 to 12 h was harmful for the activity possibly because of the extremely crowded BiOBr nanosheets and even the overlap of BiOBr nanosheets which were unfavorable for light harvesting. Meanwhile, the optimal calcination temperature was determined as 400 °C (Fig. S18) since BOB-8-400 showed the high crystallization degree without forming Bi_2O_3 impurity. More importantly, the higher activity of BOB-8-400 than that of either BOB-8-400(M) or BOB-8-400(C) films (Fig. 5) was simultaneously attributed to the following significant roles: (1) the uniform growth of vertically aligned and crisscross textured BiOBr film (Fig. S18) since the BOB-8-400 showed the high crystallization degree without forming Bi_2O_3 impurity. More importantly, the higher activity of assembled with nanosheets, (2) the stable conbination of the BiOBr film with the glass substrate *via* Bi-O-Si bond, (3) the enhanced light harvesting in the orderly assembled BiOBr nanosheets through inside multiple reflections, (4) the higher separation efficiency of photo-induced charge carriers with the stronger surface charge transfer, and (5) the higher adsorption rate mainly due to the stronger surface hydrophilicity.

In order to determine the active specie during the photocatalytic oxidation pathway of RhB degradation on BiOBr film, The ESR spectra of DMPO-$\cdot O_2^-$ and DMPO-$\cdot$OH adducts on BOB-8-400 film without RhB were shown in Fig. S19. Six characteristic peaks indicative of the DMPO-$\cdot O_2^-$ and four of the DMPO-$\cdot$OH were observed, indicating that the BiOBr film could be excited by visible lights to create photo-generated electrons and holes. More importantly, their recombination was efficiently retarded so that they could react with adsorbed oxygen and H_2O to produce $\cdot O_2^-$ and $\cdot$OH active species.[35, 36] Examination for the investigation of main active specie during the photodegradation process was also carried out *via* dissolving different trapping agents in the reaction solution before light irradiations. As shown in Fig. 6, the RhB degradation was significantly suppressed after trapping $\cdot O_2^-$ by adding BQ. Trapping photo-generated holes, electrons and $\cdot$OH with EDTA, $AgNO_3$ and TBA, respectively, exhibited much weaker restraining effect to the photodegradation rate. It could be discovered that the $\cdot O_2^-$ radical was the main active specie during the photodegradation process, in accordance with the previous work.[14]

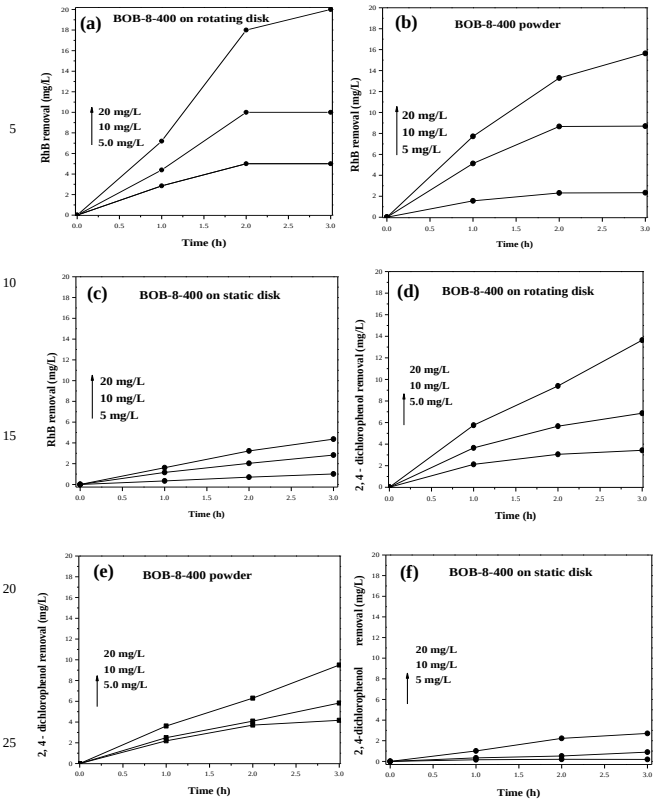

Fig. 7 RhB photocatalytic degradation of (a) BOB-8-400 on rotating disk, (b) BOB-8-400 powder obtained by scraping BiOBr film from the glass substrate of BOB-8-400 and (c) BOB-8-400 on static disk, and 4-dichlorophenol photocatalytic degradation of (d) BOB-8-400 on rotating disk, (e) BOB-8-400 powder obtained by scraping BiOBr film from the glass substrate in BOB-8-400 and (f) BOB-8-400 on static disk. Reaction conditions: four glass plates (each size = 2.5 × 2.2 cm) coated with catalysts on the disk, 55 mL RhB or 4-dichlorophenol aqueous solution with different concentration, reaction temperature = 30 °C, one 300 W Xe lamp (light intensity = 300 mW/cm^2, λ > 420 nm), rotating speed = 90 rpm.

Fig. 7 revealed that, during the visible-light-driven photocatalytic degradation of RhB and 2, 4-dichlorophenol, BOB-8-400 on the rotating disk exhibited much higher activity than either BOB-8-400 powder immersed in the solution obtained by scraping BiOBr film from the glass substrate in BOB-8-400 or BOB-8-400 on the static disk. Meanwhile, it was also found that BOB-8-400 on the rotating disk displayed much more enhancement in photocatalytic activity than others with the increase of RhB concentration. However, the enhancement in the activity of BOB-8-400 on the rotating disk was much lower during the photocatalytic degradation of 2, 4-dichlorophenol. These results demonstrated that light shielding effect from the solution could be completely removed by rotating the disk[37, 38] since the average thickness of liquid film on the disk surface was only about 75 μm at the rotating speed of 90 rpm[20, 39], leading to the enhanced photocatalytic activity. Taking into account that the photocatalytic reaction was the first order with the respect to the concentration of either one of the above two organic pollutants[37], it was found that both BOB-8-400 powder and BOB-8-400 on the static disk showed the decreased activities with the increasing RhB concentration,

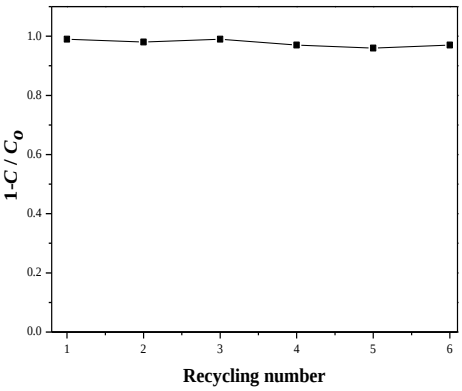

Fig. 8 Recycling test of different films. Reaction conditions: four glass plates (each size = 2.5 × 2.2 cm) coated with catalysts on the disk, 55 mL 10.0 mg/L RhB aqueous solution, reaction time = 3 h, reaction temperature = 30 °C, one 500 W Xe lamp (light intensity = 300 mW/cm^2, λ > 420 nm), rotating speed = 90 rpm.

mainly due to the enhanced light shielding with the increased solution color. For comparison, the photodegradation process of colorless 2, 4-dichlorophenol solution was involved in the much weaker light shielding effect and thus the 2, 4-dichlorophenol concentration had little influence on the activity of either BOB-8-400 powder or BOB-8-400 on the static disk. Additionally, the effect of dye sensitization could be excluded during the degradation of colorless 2, 4-dichlorophenol. Thus, the present photocatalytic reactor with photocatalyst coated on a rotating disk was more efficient in degradation of organic dyes by diminishing light shielding effect from color solution, especially with high concentration of dyes. Besides, the present reactor could also be used for photocatalytic degradation of other dye pollutants like MO and MB in aqueous solution under visible light irradiation (see Fig. S20).

More importantly, BOB-8-400 on the rotating disk exhibited strong durability. As shown in Fig. 8, no significant decrease in activity was observed after being reused repetitively for 6 times. On one hand, the leaching of BiOBr photocatalyst from the disk owing to the strong interaction between BiOBr film and the glass substrate. Meanwhile, the BiOBr film might be rinsed frequently by rotating the disk, which could efficiently inhibit the deactivation by the adsorbed impurities.

4. Conclusions

A facile solvothermal approach was developed for the preparation of BiOBr film on the pretreated soda glass substrate with the assistance of [C_{16}mim]Br IL. The strong combination of uniformly assembled BiOBr nanosheets with the glass substrate was formed *via* the Bi-O-Si bond. The unique film morphology comprised of ordered assembly of BiOBr nanosheets favored light harvesting through inside multiple reflections. Meanwhile, the high separation efficiency of photo-induced charge carriers with the strong surface charge transfer and the fast adsorption rate were achieved. As a result, the BiOBr photocatalytic film utilized in the rotating disk reactor, which could effectively avoid light shielding from color solution by rotating the disk, presented the enhanced activity and strong stability for the visible-light photodegradation of dyeing compounds. Additionally, the $\cdot O_2^-$ radical was determined as the main active specie during the photodegradation process. The BiOBr film in rotating disk reactor supplied a promising way for the practical

application in the color wastewater treatment by directly utilizing solar light.

ACKNOWLEDGMENTS

This work is supported by National Natural Science Foundation of China (21261140333, 21237003 and 21207091), Program for Changjiang Scholars and Innovative Research Team in University (IRT1269) and International Joint Laboratory on Resource Chemistry (IJLRC). Dr. Xiao Wei in Shanghai Jiaotong University is acknowledged for the assistance of SPS measurement.

References

1 X. B. Chen and S. S. Mao, *Chem. Rev.*, 2007, 107, 2891-2959.
2 Y. Lu, H. T. Yu, S. Chen, X. Quan and H. M. Zhao, *Environ. Sci. Technol.*, 2012, 46, 1724-1730.
3 H. J. Zhang, G. H. Chen and D. W. Bahnemann, *J. Mater. Chem.*, 2009, 19, 5089-5121.
4 R. Su, R. Bechstein, J. Kibsgaard, R. T. Vang and F. Besenbacher, *J. Mater. Chem.*, 2012, 22, 23755-23758.
5 M. D. Hernandez-Alonso, F. Fresno, S. Suarez and J. M. Coronado, *Energy Environ. Sci.*, 2009, 2, 1231-1234.
6 Y. N. Huo, M. Miao, Y. Zhang, J. Zhu and H. X. Li, *Chem. Commun.*, 2011, 47, 2089-2091.
7 W. D. Wang, F. Q. Huang and X. P. Lin, *Scripta Mater.*, 2007, 56, 669-672.
8 J. Zhang and C. C. Tang, *Chem. Mater.*, 2008, 20, 2937-2941.
9 L. Q. Ye, J. Y. Liu and Z. Jiang, *Appl. Catal. B*, 142 (2013) 1-7.
10 Y. Wang, Z. Q. Shi and C. M. Fan, *J. Solid State Chem.*, 2013, 199, 224-229.
11 J. Y. Xiong, Q. S. Dong and T. Wang, *RSC Adv.*, 2014, 4, 583-589.
12 Z. Jiang, F. Yang, G. D. Yang, L. Kong, M. O. Jones, T. C. Xiao and P. P. Edwards, *J. Photochem. Photobio. A*, 2010, 212, 8-13.
13 J. Henle, P. Simon, A. Frenzel, S. Scholz and S. Kaskel, *Chem. Mater.*, 2007, 19, 366-373.
14 Y. N. Huo, J. Zhang, M. Miao and Y. Jin, *Appl. Catal. B*, 2012, 111-112, 334-341.
15 Z. H. Ai, W. k. Ho, S. C. Lee, L. Z. Zhang, *Environ. Sci. Technol.*, 2009, 43, 4143-4150.
16 L. Zhang, X. F. Cao, X. T. Chen and Z. L. Xue, *J. Colloid. Interf. Sci.*, 2011, 354, 630-636.
17 Z. P. Yao, F. Z. Jia, S. J. Tian, C. X. Li, Z. H. Jiang and X. F. Bai, *ACS Appl. Mater. Interfaces*, 2010, 2, 2617-2622.
18 W. B. Heuer, H. L. Xia, M. Abrahamsson, Z. Zhou, S. Ardo, A. A. N. Sarjeant and G. J. Meyer, *Inorg. Chem.*, 2010, 49, 7726-7734.
19 D. S. Kim and S. Y. Kwak, *Environ. Sci. Technol.*, 2009, 43, 148-151.
20 Y. L. Xu, Y. He, X. D. Cao, D. J. Zhong and J. P. Jia, *Environ. Sci. Technol.*, 2008, 42, 2612-2617.
21 W. K. Ho, J. C. Yu and J. G. Yu, *Langmuir*, 2005, 21, 3486-3492.
22 M. Tomozawa, V. McGahay, J. M. J. Hyde, *Non-Cryst. Solids*, 1990, 123, 197-207.
23 S. A. Katsyuba, P. J. Dyson, E. E. Vandyukova, A. V. Chernova and A. Vidisoe, *Helvetica Chimica Acta*, 2004, 87, 2556-2565.
24 L. Wang, L. X. Chang, L. Q. Wei, S. Z. Xu, M. H. Zeng and S. L. Pan, *J. Mater. Chem.*, 2011, 21, 15732-15740.
25 B. Lal, S. K. Patro and S. Singh, *J. Sol-Gel Sci. Technol.*, 2010, 56, 340-344.
26 R. G. Chen, J. H. Bi, L. Wu, W. J. Wang, Z. H. Li and X. Z. Fu, *Inorg. Chem.*, 2009, 48, 19-21.
27 R. Reiche, R. Thielsch, S. Oswald and K. Wetzig, *J. Electron Spectrosc.*, 1999, 104, 161-171.
28 J. X. Xia, S. Yin, H. M. Li, H. Xu, L. Xu and Y.G. Xua, Dalton Trans. 2011, 40, 5249-5258.
29 A. M. Cao, J. S. Hu, H. P. Liang and L. J. Wan, *Angew. Chem. Int. Ed.*, 2005, 44, 4391-4395.
30 M. B. Gonzalez, A. Wu and P. M. Vilarinho, *Chem. Mater.*, 2006, 18, 1737-1744.
31 Y. L. Lu, D. Wang, T. Xie, L. Chen and Y. Lin, *Mater. Chem. Phys.*, 2011, 129, 281-287.
32 Q. D. Zhao, D. J. Wang, L. L. Peng, Y. H. Lin, M. Yang and T. F. Xie, *Chem. Phys. Lett.*, 2007, 434, 96-100.
33 L. Q. Jing, J. Wang, Y. Qu and Y. Luan, *Appl. Surf. Sci.*, 2009, 256, 657-663.
34 L. Mohapatra, K. Parida and M. Satpathy, *J. Phys. Chem. C*, 2012, 116, 13063-13070.
35 C. Hu, Y. Q. Lan, J. H. Qu, X. X. Hu and A. M. Wang, *J. Phys. Chem. B*, 2006, 110, 4066-4072.
36 C. C. Chen, Q. Wang, P. X. Lei, W. J. Song, W. H. Ma and J. C. Zhao, *Environ. Sci. Technol.*, 2006, 40, 3965-3970.
37 K. Li, Y. He, Y. L. Xu, Y. L. Wang and J. P. Jia, *Environ. Sci. Technol.*, 2011, 45, 7401-7407.
38 Y.N. Huo, X. F. Chen, J. Zhang, G. F. Pan, J. P. Jia and H. X. Li, *Appl. Catal. B.*, 2014, 148-149, 550-556.
39 J. A. Zeevalkink, P. Kelderman and C. Bouelhouwer. *Water Res.*, 1978, 12, 577-581.

Table of contents entry：

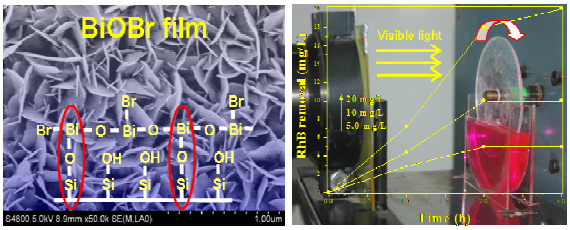

BiOBr visible-light photocatalytic films utilized in rotating disk reactor have achieved improved photoactivity for the degradation of color organics.